Supplement of Atmos. Chem. Phys., 24, 5199–5219, 2024
https://doi.org/10.5194/acp-24-5199-2024-supplement
© Author(s) 2024. CC BY 4.0 License.

Atmospheric Chemistry and Physics
Open Access

Supplement of

Dust storms from the Taklamakan Desert significantly darken snow surface on surrounding mountains

Yuxuan Xing et al.

Correspondence to: Wei Pu (puwei@lzu.edu.cn)

The copyright of individual parts of the supplement might differ from the article licence.

S1 Method

S1.1 Attribution of the spatial variation in snow albedo reduction

As noted above, the snow albedo reduction depends mainly on the dust content, snow optical effective radius (R_{eff}), snow depth (SD) and solar zenith angle (SZ). Snow optical effective radius and snow depth can be categorized as the snow properties (SP). Here we choose these three variables to discuss their fractional contributions to the spatial variability in snow albedo reduction. $\Delta\alpha$ can be expressed as

$$\Delta\alpha = f(\text{dust}, \text{SP}, \text{SZ}). \quad \text{(S1)}$$

The spatial variability about snow albedo reduction due to dust can be described as

$$\Delta\alpha(\text{dust}) = f(\text{dust}, \overline{\text{SP}}, \overline{\text{SZ}}), \quad \text{(S2)}$$

where $\overline{\text{SP}}$ and $\overline{\text{SZ}}$ indicate spatial-mean values of SP, and SZ. Similarly, we can obtain the following equations:

$$\Delta\alpha(\text{SP}) = f\left(\overline{\text{dust}}, \text{SP}, \overline{\text{SZ}}\right), \quad \text{(S3)}$$

$$\Delta\alpha(\text{SZ}) = f\left(\overline{\text{dust}}, \overline{\text{SP}}, \text{SZ}\right). \quad \text{(S4)}$$

We fit the $\Delta\alpha$ based on multiple linear regression, we can express it as

$$\Delta\alpha_{\text{fit}} = a \times \Delta\alpha(\text{dust}) + b \times \Delta\alpha(\text{SP}) + c \times \Delta\alpha(\text{SZ}), \quad \text{(S5)}$$

where $\Delta\alpha_{\text{fit}}$ is the fitted snow albedo reduction, and *a*, *b*, *c* represent the regression coefficients. As a result, we can use $\Delta\alpha_{\text{fit}}$ to replace $\Delta\alpha$ to access the contribution to spatial variation of individual variables, Eq. (14) can be written as follows:

$$\Delta\alpha_{\text{fit}} - \overline{\Delta\alpha_{\text{fit}}} = a \times (\Delta\alpha(\text{dust}) - \overline{\Delta\alpha(\text{dust})}) + b \times (\Delta\alpha(\text{SP}) - \overline{\Delta\alpha(\text{SP})}) + c \times (\Delta\alpha(\text{SZ}) - \overline{\Delta\alpha(\text{SZ})}), \quad \text{(S6)}$$

where we use $\Delta\alpha_{\text{fit}} - \overline{\Delta\alpha_{\text{fit}}}$ represent snow albedo reduction anomaly ($\Delta\alpha_{\text{fit}}^{\text{anomaly}}$). After, Eq. (15) can be written as

$$\Delta\alpha_{\mathrm{fit}}^{\mathrm{anomaly}} = \mathrm{a}\times\Delta\alpha_{\mathrm{anomaly}}(\mathrm{dust})+\mathrm{b}\times\Delta\alpha_{\mathrm{anomaly}}(\mathrm{SP})+\mathrm{c}\times\Delta\alpha_{\mathrm{anomaly}}(\mathrm{SZ}). \quad (\mathrm{S7})$$

According to Pu et al. (2019) and Cui (2021), the fractional contribution of dust to the spatial variability in snow albedo reduction (F_{dust}) can be written as

$$F_{\mathrm{dust}}=\frac{1}{n}\sum_{i=1}^{n}\frac{(a\times\Delta\alpha_{\mathrm{anomaly}}(\mathrm{dust}))^{2}}{X_i}, \quad (\mathrm{S8})$$

$$X_i=\left(a\times\Delta\alpha_{\mathrm{anomaly}}(\mathrm{dust})_i\right)^2+\left(b\times\Delta\alpha_{\mathrm{anomaly}}(\mathrm{SP})_i\right)^2+\left(c\times\Delta\alpha_{\mathrm{anomaly}}(\mathrm{SZ})_i\right)^2. \quad (\mathrm{S9})$$

where n represent the length of the data set. Similarly, we can get the F_{SP} and F_{SZ}.

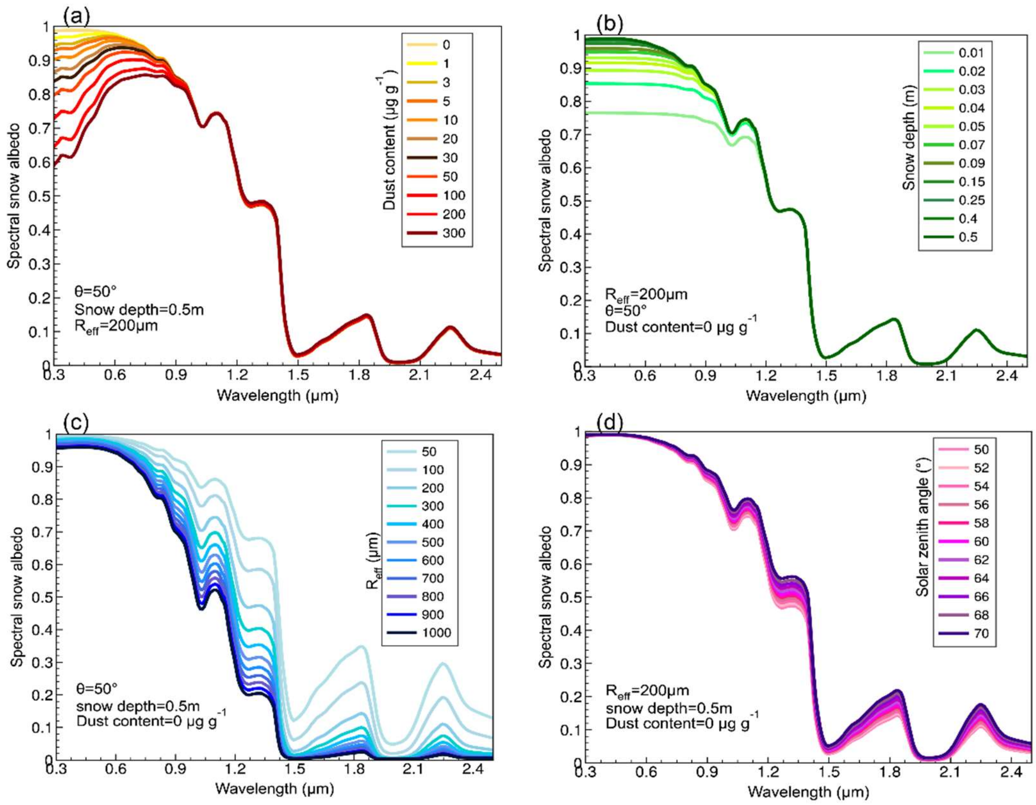

Figure S1. Variations in spectral snow albedo due to (a) dust content (μg g^{-1}), (b) snow depth (m), (c) snow grain size (μm), and (d) solar zenith angle (∘) while the other three parameters are kept constant.

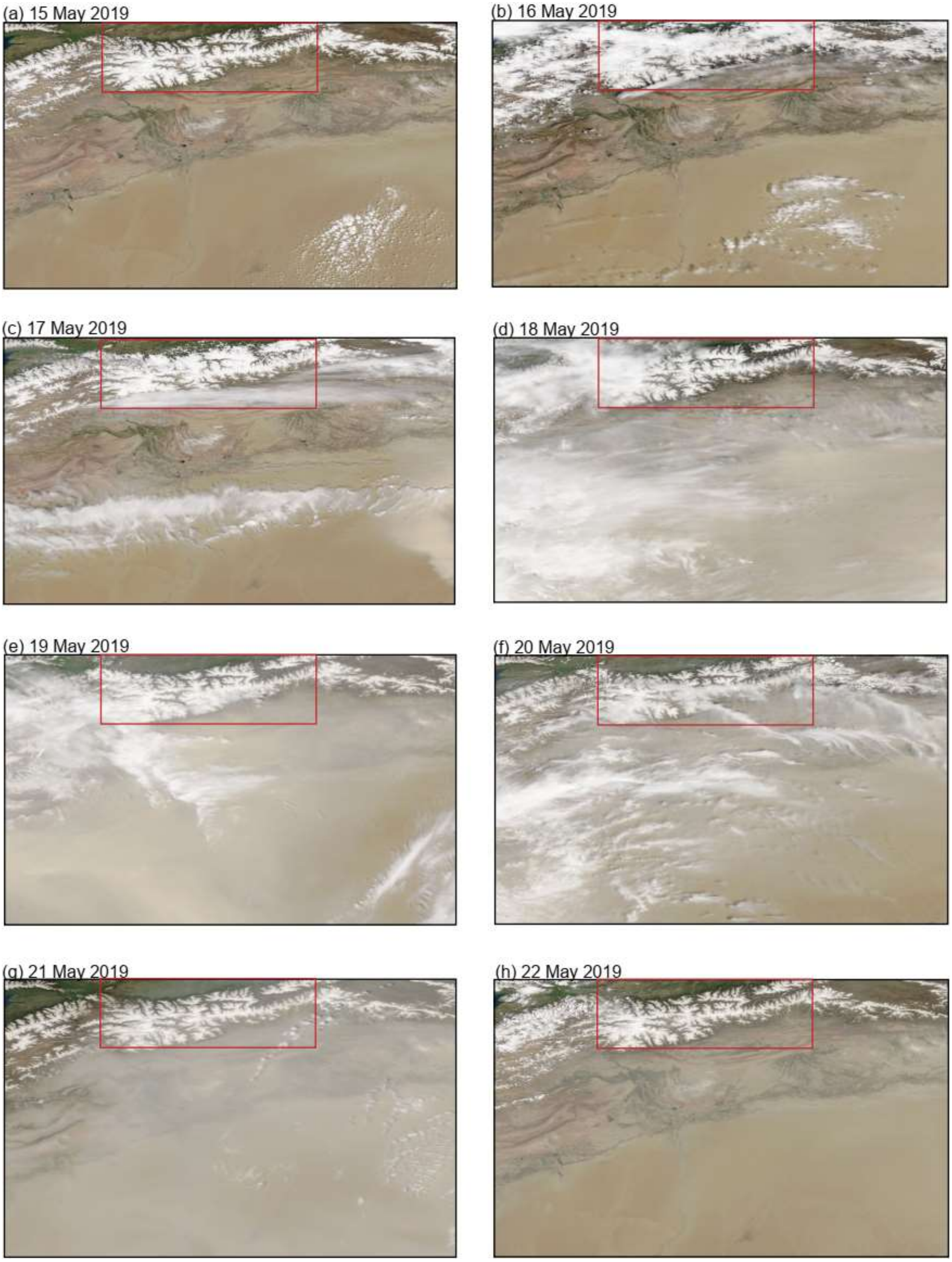

Figure S2. Satellite observations during the 15–22 May 2019 severe dust event across the Tien Shan (a-h). Satellite images (a-h) are from Terra/MODIS (https://worldview.earthdata.nasa.gov).

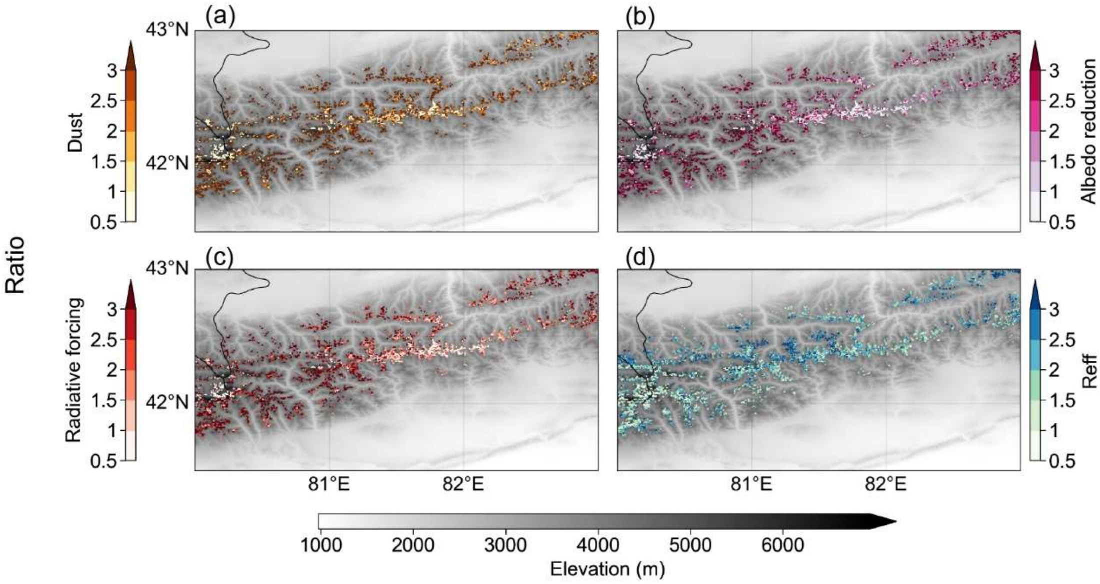

Figure S3. Spatial distribution of the ratios between 15 May 2019 and 22 May 2019 of (a) dust, (b) albedo reduction, (c) radiative forcing and (d) R_{eff}. The background images in (a-d) show the elevation of Tien Shan.

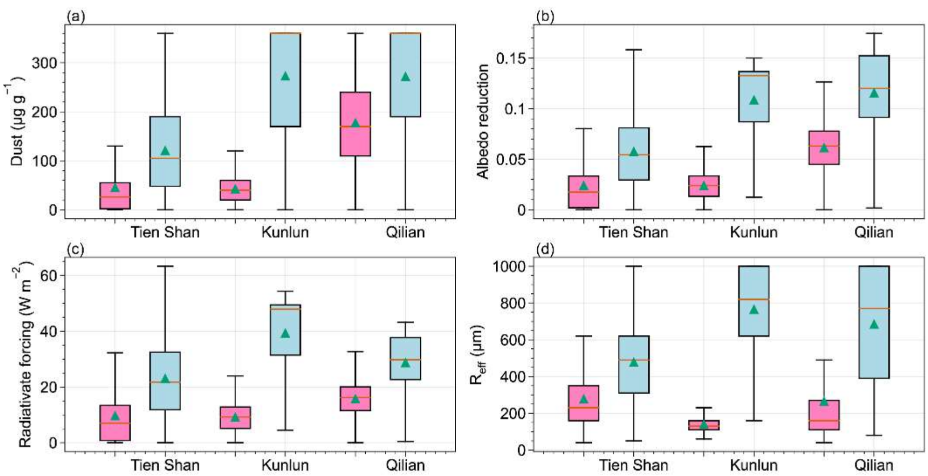

Figure S4. Statistics for regionally averaged (a) dust, (b) albedo reduction, (c) radiative forcing and (d) R_{eff} for Tien Shan, Kunlun Mountains and Qilian Mountains. The pink color shows 15 May, 2019, 23 August, 2019 and 01 November, 2012 before the dust storm in three regions. The blue color shows 22 May, 2019, 06 Sep, 2019 and 04 November, 2012 after the dust storm in three regions. The boxes denote the 25th and 75th quantiles, and the horizontal lines represent the 50th quantiles (medians); the averages are shown as blue triangle; the whiskers denote the 5th and 95th quantiles.

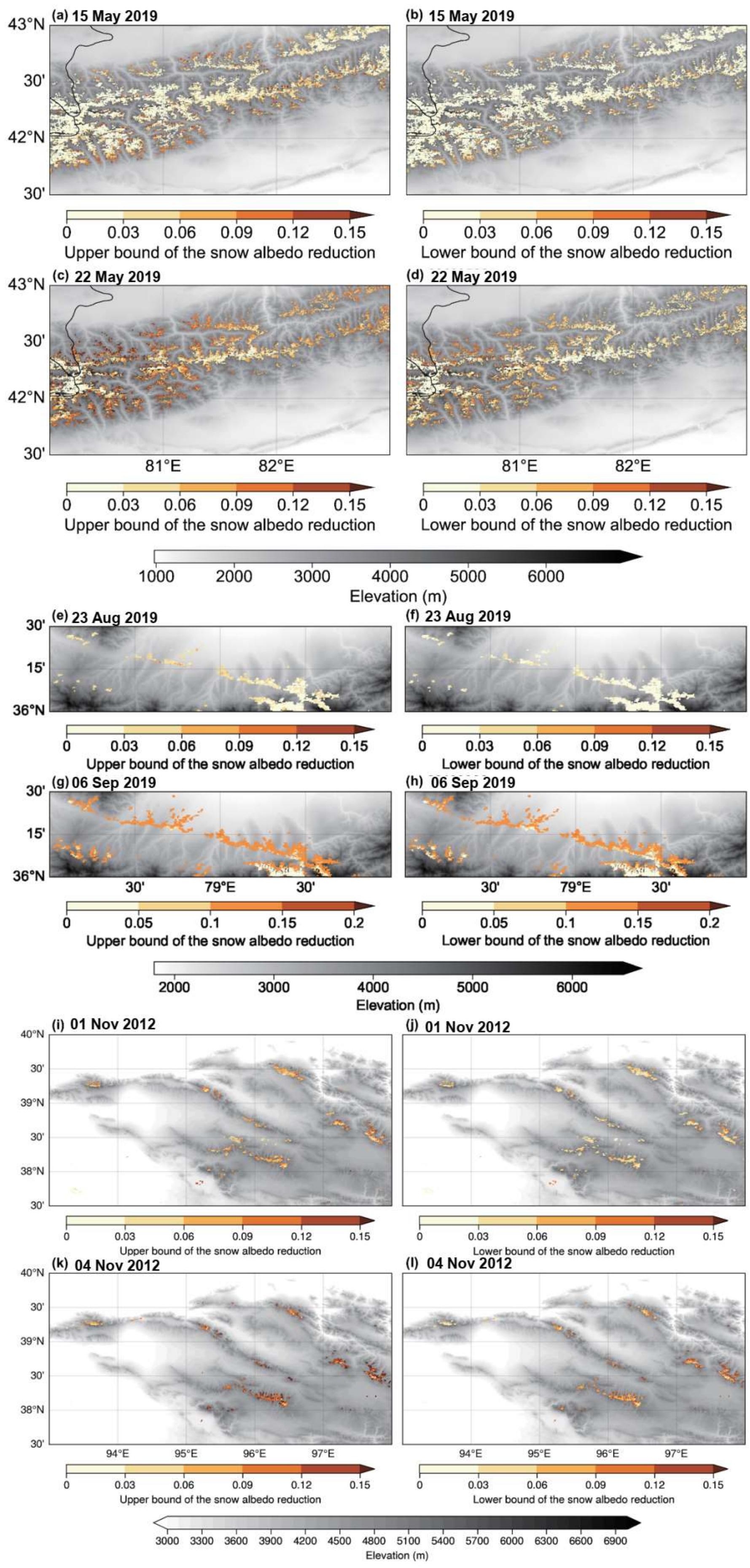

(a) 15 May 2019
(b) 15 May 2019
43°N
30'
42°N
30'
0 0.03 0.06 0.09 0.12 0.15
Upper bound of the snow albedo reduction
Lower bound of the snow albedo reduction
(c) 22 May 2019
(d) 22 May 2019
81°E
82°E
1000 2000 3000 4000 5000 6000
Elevation (m)
(e) 23 Aug 2019
(f) 23 Aug 2019
30'
15'
36°N
(g) 06 Sep 2019
(h) 06 Sep 2019
30'
79°E
30'
0 0.05 0.1 0.15 0.2
2000 3000 4000 5000 6000
Elevation (m)
(i) 01 Nov 2012
(j) 01 Nov 2012
40°N
30'
39°N
30'
38°N
30'
(k) 04 Nov 2012
(l) 04 Nov 2012
94°E
95°E
96°E
97°E
3000 3300 3600 3900 4200 4500 4800 5100 5400 5700 6000 6300 6600 6900
Elevation (m)

Figure S5. The overall lower bound and upper bound of the uncertainty value of snow albedo reduction retrieval due to atmospheric correction in Tien Shan (a-d), Kunlun Mountains (e-h) and Qilian Mountains (i-l).

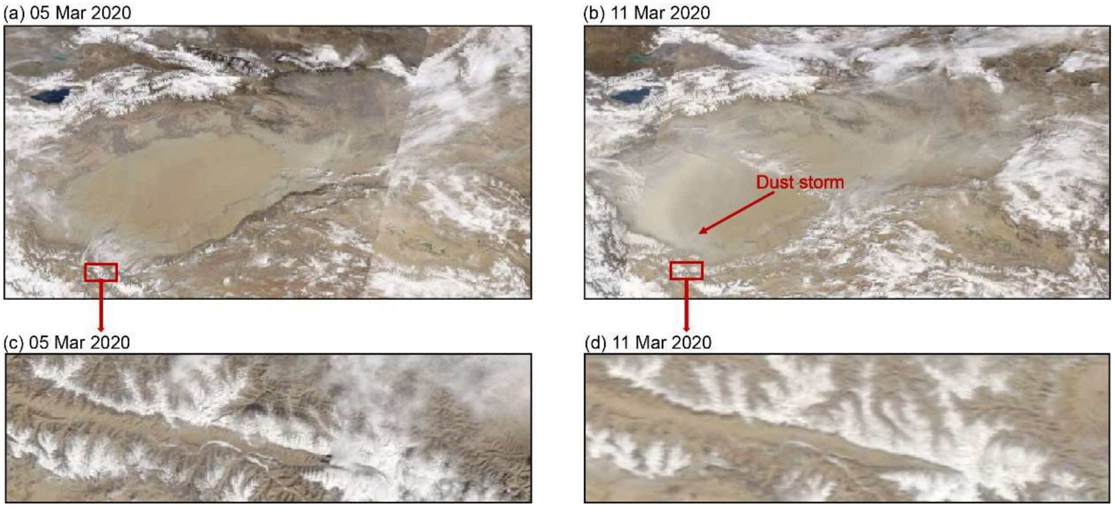

Figure S6. Satellite observations during the 05–11 March 2020 severe dust event across the Kunlun Mountains. (a, c) Terra/MODIS satellite true-color images acquired on 05 March 2020, prior to the dust storm. (b, d) Terra/MODIS satellite images acquired on 11 March 2020, with significant snow darkening across the Kunlun Mountains after the dust storm. Satellite images (a-d) are from Terra/MODIS (https://worldview.earthdata.nasa.gov).

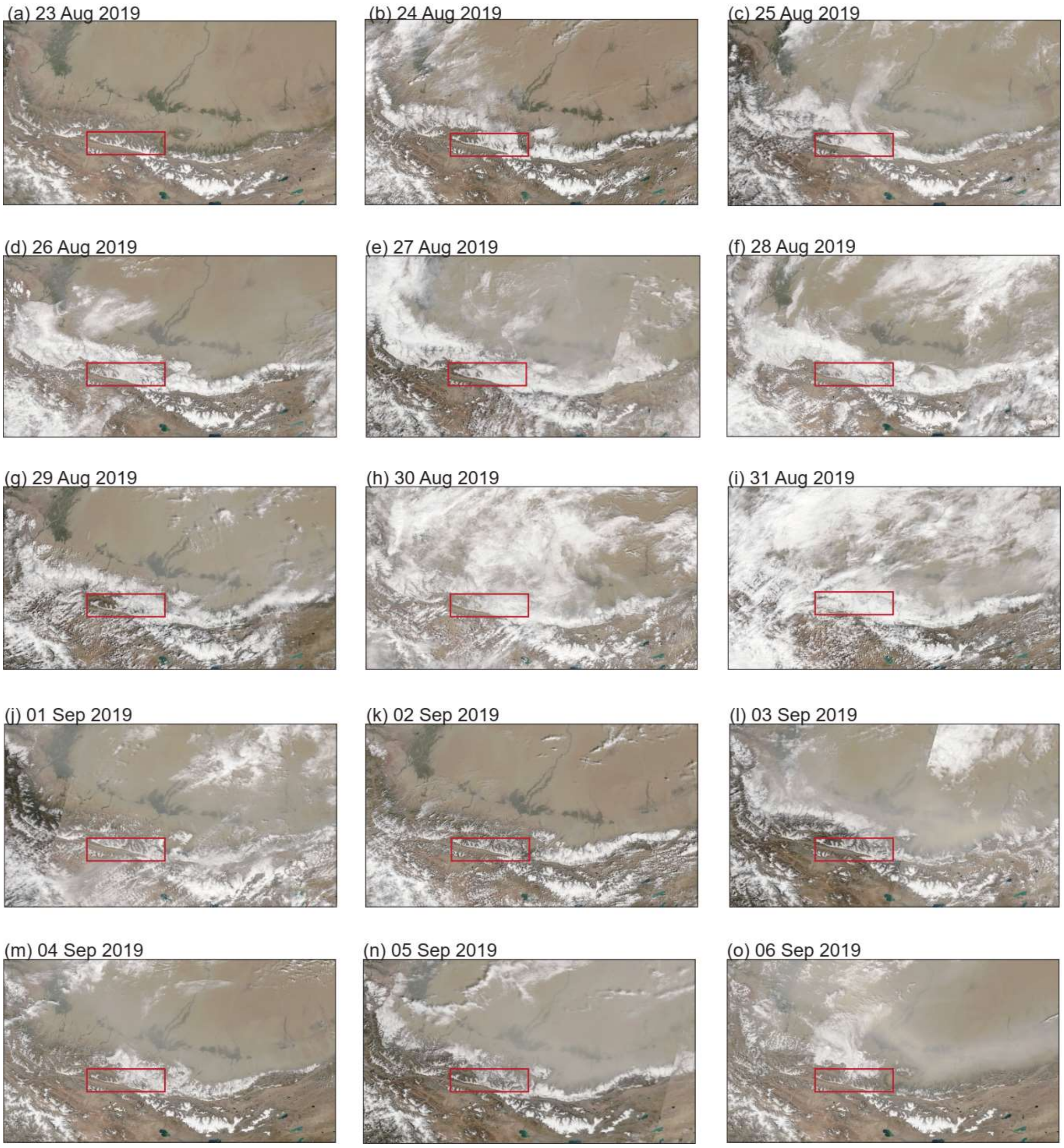

Figure S7. Satellite observations during the 23 August to 06 September 2019 severe dust event across the Kunlun Mountains (a-o). Satellite images (a-o) are from Terra/MODIS (https://worldview.earthdata.nasa.gov).

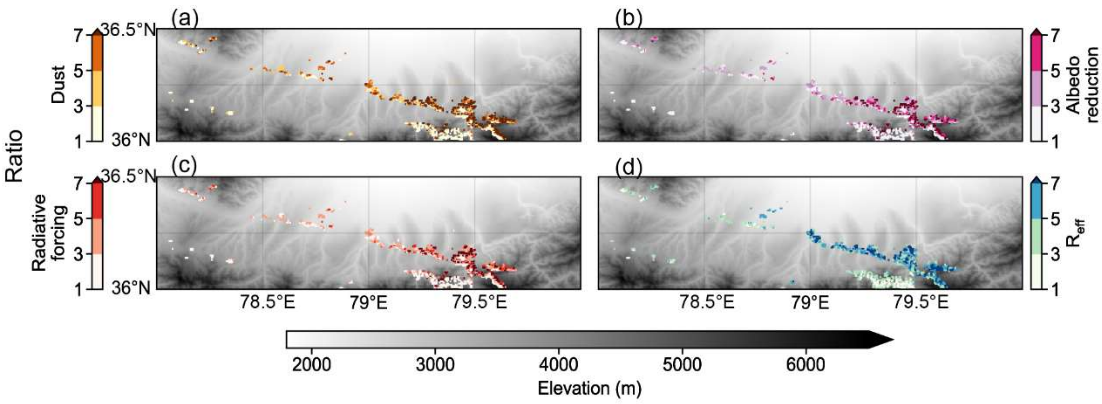

Figure S8. Spatial distribution of the ratio between 23 Aug 2019 and 06 Sep 2019 of (a) dust, (b) albedo reduction, (c) radiative forcing and (d) R_{eff}. The background images in (a-d) show the elevation of Kunlun Mountains.

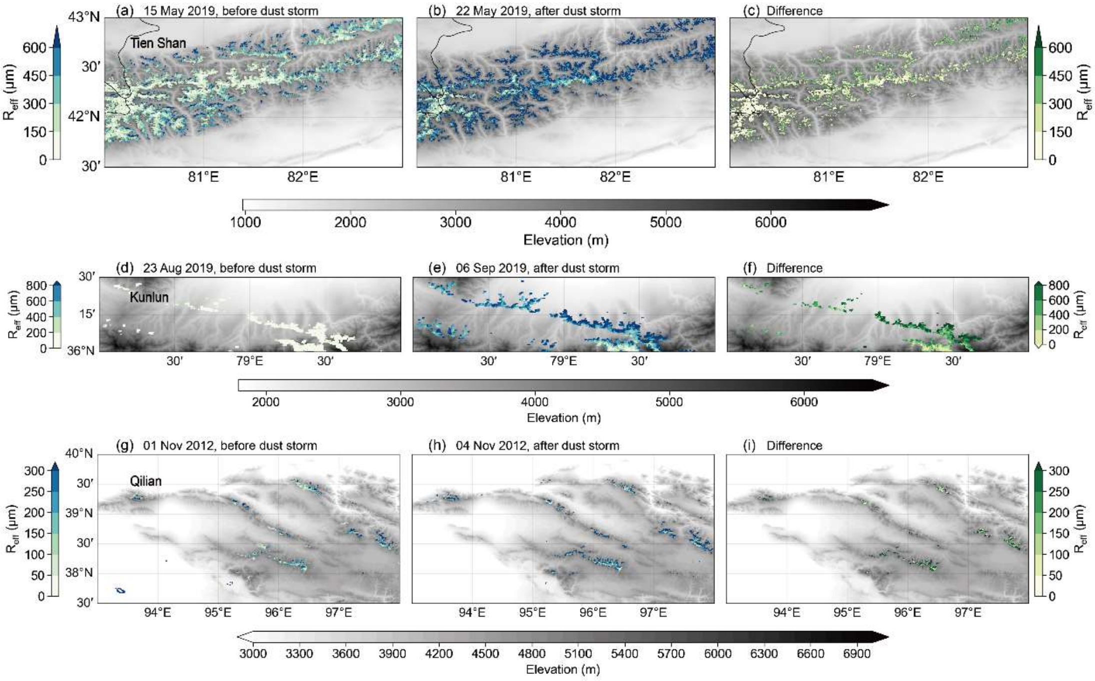

Figure S9. Spatial distributions of the average values and differences of R_{eff} across the (a-c) Tien Shan, (d-f) Kunlun Mountains and (g-i) Qilian Mountains, respectively.

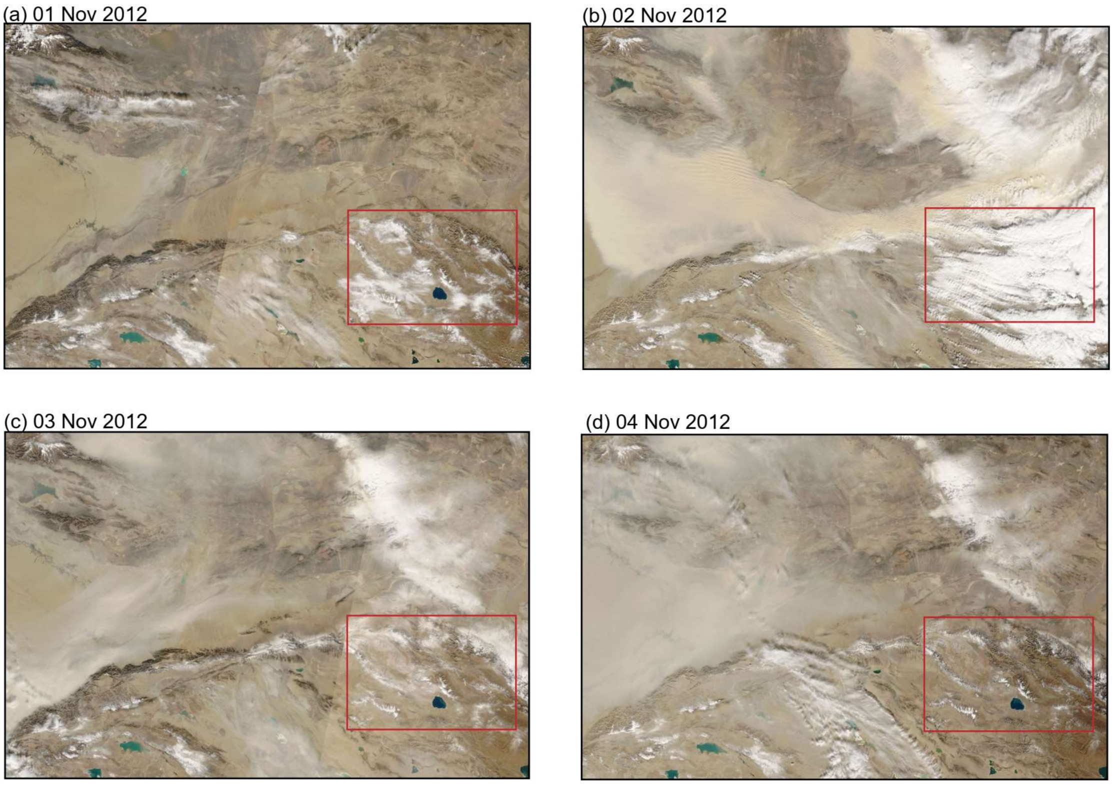

Figure S10. Satellite observations during the 01–04 November 2012 severe dust event across the Qilian Mountains (a-d). Satellite images (a-d) are from Terra/MODIS (https://worldview.earthdata.nasa.gov).

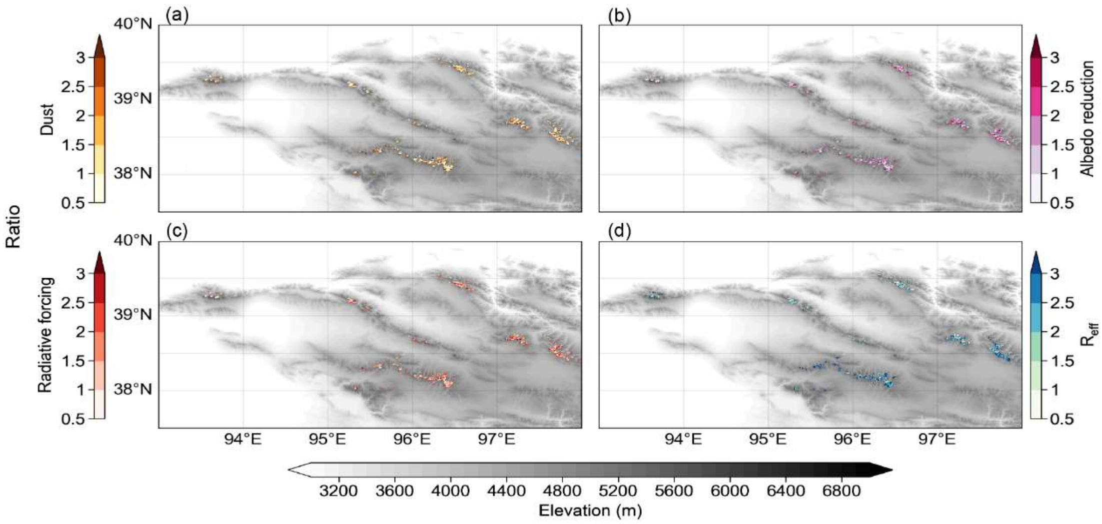

Figure S11. Spatial distribution of the ratio between 01 Nov 2012 and 04 Nov 2012 of (a) dust, (b) albedo reduction, (c) radiative forcing and (d) R_{eff}. The background images in (a-d) show the elevation of Qilian Mountains.

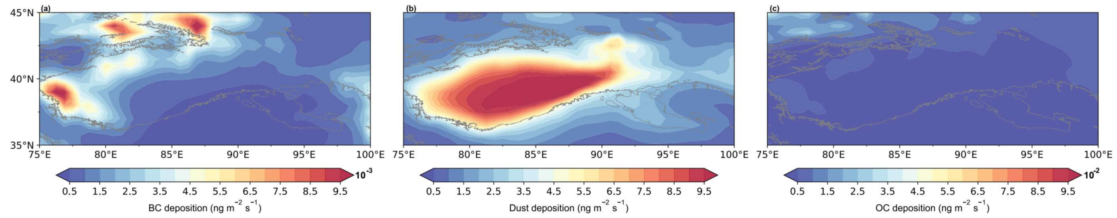

Figure S12. Spatial distributions of the averaged MERRA-2 (a) BC, (b) dust and (c) OC deposition rate from March to August 2019.

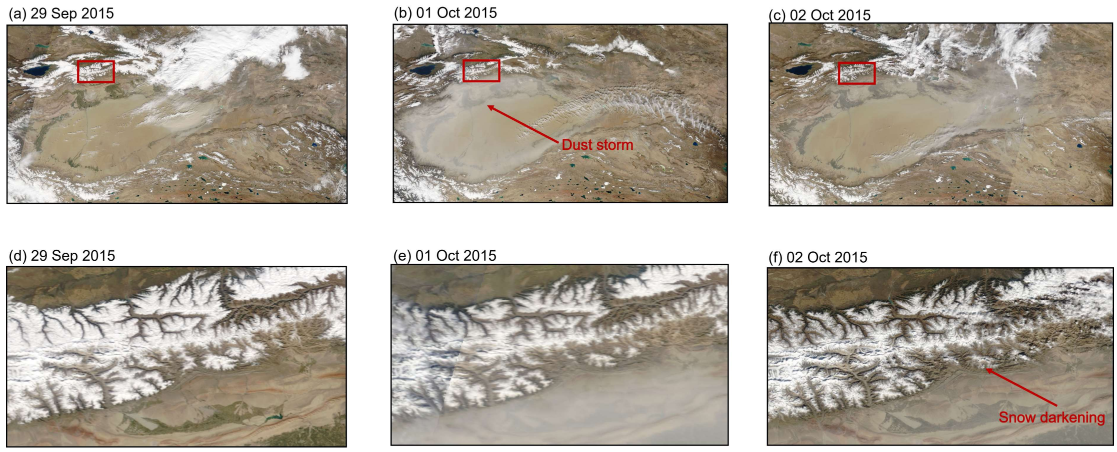

Figure S13. Satellite observations during the 29 September to 02 October 2015 severe dust event across the Tien Shan (a-f). Satellite images (a-f) are from Terra/MODIS (https://worldview.earthdata.nasa.gov).

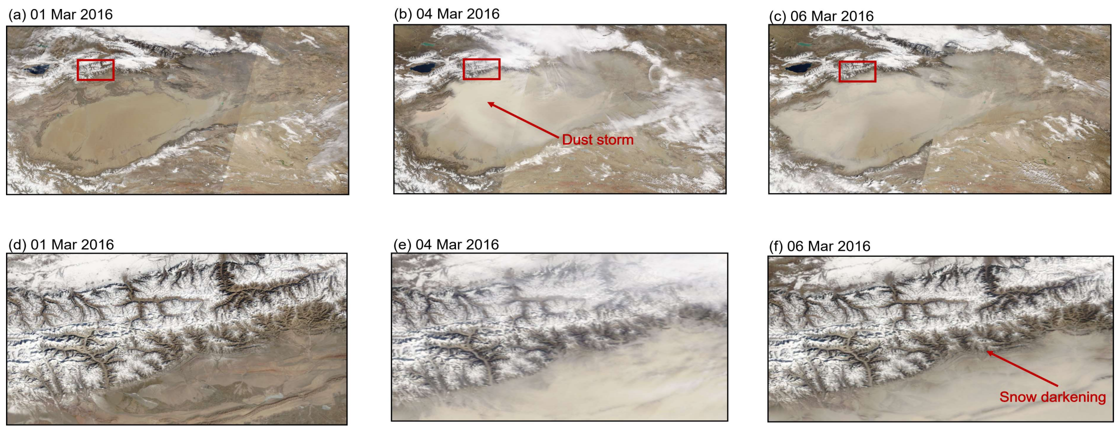

Figure S14. Satellite observations during the 01–06 March 2016 severe dust event across the Tien Shan (a-f). Satellite images (a-f) are from Terra/MODIS (https://worldview.earthdata.nasa.gov).

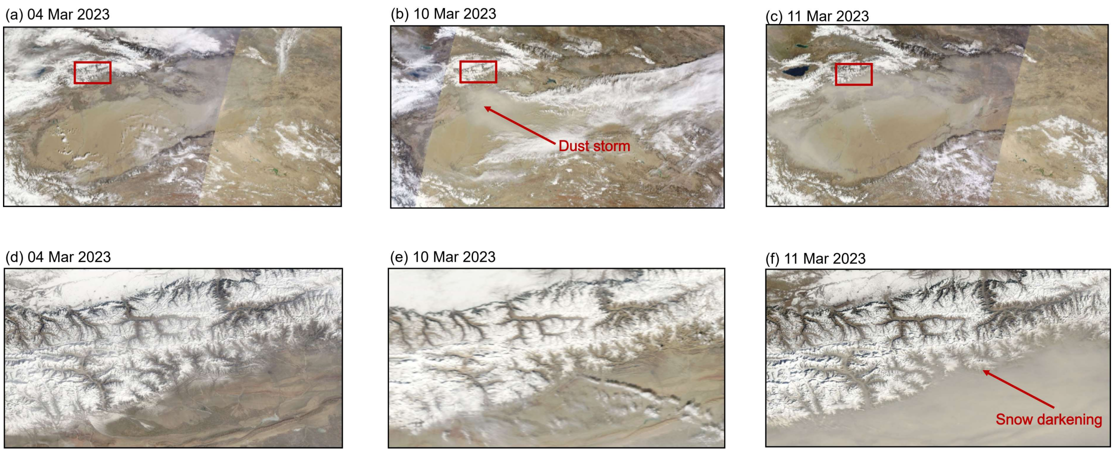

Figure S15. Satellite observations during the 04–11 March 2023 severe dust event across the Tien Shan (a-f). Satellite images (a-f) are from Terra/MODIS (https://worldview.earthdata.nasa.gov).

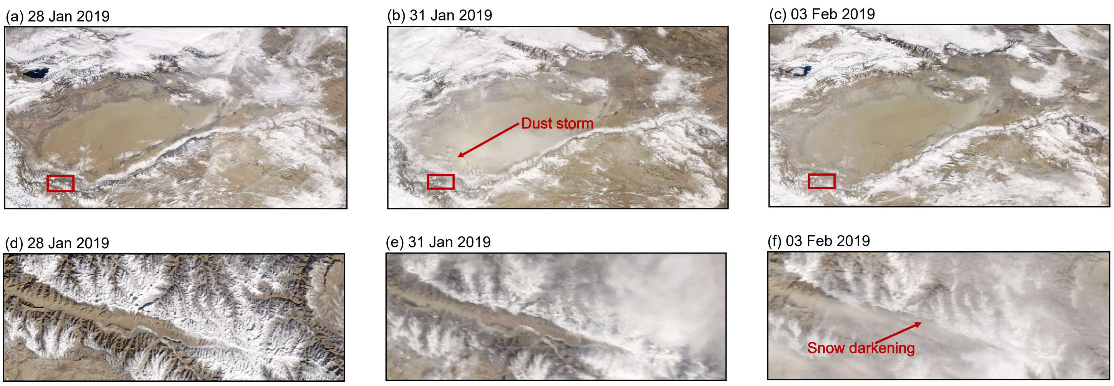

Figure S16. Satellite observations during the 28 January to 03 February 2019 severe dust event across the Kunlun Mountains (a-f). Satellite images (a-f) are from Terra/MODIS (https://worldview.earthdata.nasa.gov).

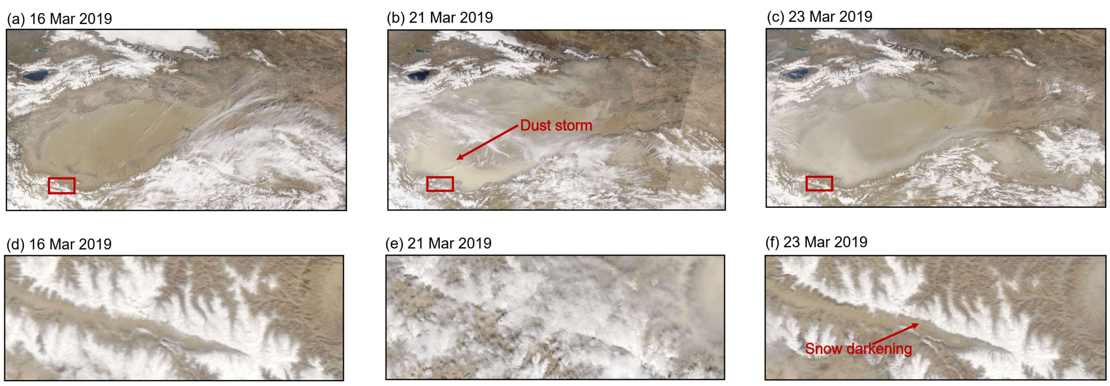

Figure S17. Satellite observations during the 16–23 March 2019 severe dust event across the Kunlun Mountains (a-f). Satellite images (a-f) are from Terra/MODIS (https://worldview.earthdata.nasa.gov).

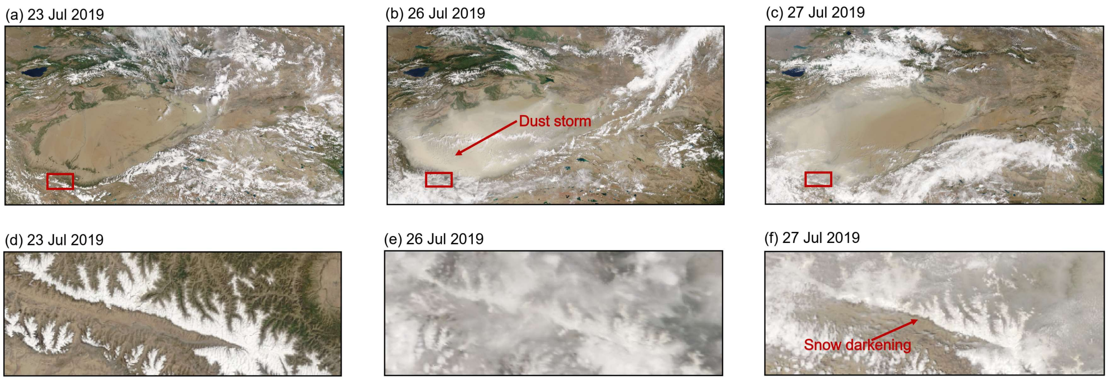

Figure S18. Satellite observations during the 23–27 July 2019 severe dust event across the Kunlun Mountains (a-f). Satellite images (a-f) are from Terra/MODIS (https://worldview.earthdata.nasa.gov).

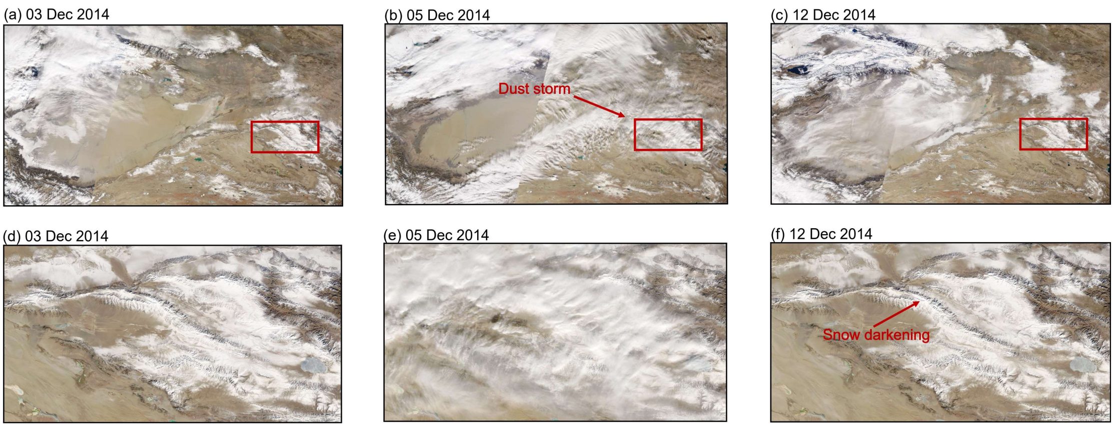

Figure S19. Satellite observations during the 03–12 December 2014 severe dust event across the Qilian Mountains (a-f). Satellite images (a-f) are from Terra/MODIS (https://worldview.earthdata.nasa.gov).

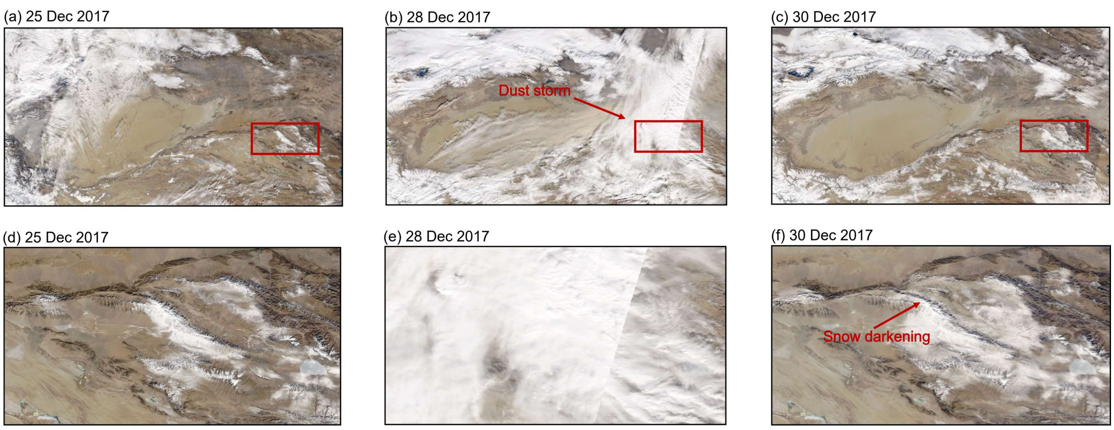

Figure S20. Satellite observations during the 25–30 December 2017 severe dust

event across the Qilian Mountains (a-f). Satellite images (a-f) are from Terra/MODIS (https://worldview.earthdata.nasa.gov).

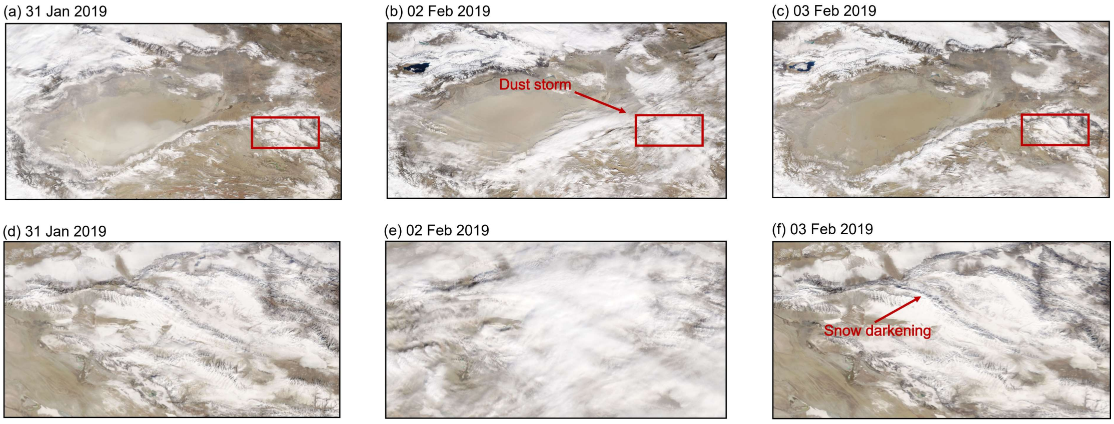

Figure S21. Satellite observations during the 31 January to 03 February 2019 severe dust event across the Qilian Mountains (a-f). Satellite images (a-f) are from Terra/MODIS (https://worldview.earthdata.nasa.gov).